Heuristic Dynamic Programming Guidance for Circular Trajectories with Impact Angle Constraints

Hong-Xia Li[1] and Yuan-Li Cai[2,*]

[1]*Jiangsu University, 212013, Jiangsu, People's Republic of China*

[2]*Xi'an Jiaotong University, 710049, Shaanxi, People's Republic of China*

Abstract: This paper proposes a new optimal guidance law around circular trajectories to control impact angle constraints in three-point guidance mode. The guidance law employs a presented heuristic dynamic programming (HDP) algorithm to realize close loop and provide optimized weighting matrices. To obtain the accurate optimized matrices fast, a multi-search mode particle swarm optimization (MMPSO) method is used. Moreover, the stationary target can be attacked successfully under the presented guidance, and the less control effort and smoother trajectories are well guaranteed. Additionally, the effectiveness and applicability of our proposed guidance scheme are explicitly verified through simulation tests.

Keywords: Circular trajectories, HDP, Three-point guidance mode, MMPSO.

1. INTRODUCTION

The solution of conventional dynamic programming (DP) optimal guidance law is guaranteed by Bellman's optimality principle. However, the guidance law heavily depends on choosing appropriate weighting matrices, which can reduce the weighted quadratic sum of the short period mode variables during the terminal flight. Therefore, the guidance problem base on DP can be seen as how to select the weighting matrices to fulfill the attack of target.

To achieve the satisfying weighting matrices, many optimization algorithms have been designed. Particle swarm optimization (PSO) algorithm was firstly proposed in [1, 2]. As this method can be implemented easily and had perfect performance on many optimization problems, many scholars used it to solve different problems. For example, Ref. [3] employed it to design adaptive particle filter for the estimation of state of charge, Ref. [4] achieved snowpack permittivity retrieval by this algorithm, and Ref [5] planned underwater manipulator trajectory using it. Moreover, many variants of PSO algorithm were presented, e.g., multi-objective PSO in [6, 7], Multi-search PSO in [8], and group merging PSO in [9]. Although these methods can realize the optimization of parameters by introducing new particles during the process, the update mode of particle velocity and position was relatively single, so that theconvergence of particles was slow. To improve the levels of search efficiency and accuracy, MMPSO algorithm [10] was designed. The method had faster convergence and deeper search depth than other PSO. Due to that, this algorithm can satisfy the high requirements for time and precision in guidance. Therefore, the presented HDP guidance law will employ it to optimize the weight matrices on three-point guidance mode which is more realistic in the attack of fixed target.

To fulfill optimal guidance, many scholars designed different laws based on time-to-go estimation. Ref. [11] firstly predicted time-to-go and used it to design optimal guidance law. After that, a guidance algorithm based on dual control was proposed in [12] to achieve the interception of target and the estimation of time-to-go, but this guidance law was invalid when interceptor was away from homing triangle. To address the linear quadratic optimal control problem in guidance process, Ref. [13] designed an energy cost weighting matrix and made it as the function of time-to-go. However, different ways had different accuracy levels, and the guidance precision can be affected by the inaccurate estimate. Aside from that, these laws did not consider impact angle constraint which can guide aircraft to hit target with desired angle and achieve maximum damage effects. This is greatly essential in some cases, e.g., the attack of aircraft carrier or tank. To avoid the problems, Ref. [14] proposed an optimal guidance law based on a parameterized solution. This guidance law not only can realize the control of impact angle, but also can avoid the prediction of time-to-go. Ref. [15] presented such a guidance law based on neural-network to resolve the problem of nonlinear optimal terminal guidance with impact angle constraints. Ref. [16] also designed an optimal guidance using sliding mode control theory to achieve the attack of maneuvering target with desired impact

*Address correspondence to this author at the Institute of Control Engineering, Xi'an Jiaotong University, People's Republic of China;
E-mail: ylicai@mail.xjtu.edu.cn

angle. Moreover, Ref. [17] designed such a guidance law to fulfill the control of both impact time and angle, and the need for time-to-go estimation was eliminated. Ref. [18] addressed the nonlinear optimal guidance problem with impact-time and impact-angle constraints without estimating the time-to-go. On the other hand, some guidance laws were designed based on programming method. Ref. [19] researched a guidance law using model predicted static programming (MPSP). Given the programming method, Ref. [20] proposed a law considering impact angle constraint towards air-to-ground interceptors. Ref. [21] presented a law for air-to-air interceptors in three-dimensional space. Ref. [22] proposed a generalized MPSP and employed it to design an impact angle constrained guidance for air-to-surface interceptors. However, these laws based on static programming can only realize the suboptimal control of guidance system, as the required parameters were optimized by static scheme. To resolve the problem, the guidance based on heuristic dynamic programming was designed in this paper to attack stationary target and satisfy the impact angle constraint.

With respect to the previously published optimal guidance laws, the proposed guidance scheme acquires several advantages: (1) the stationary target can be effectively attacked, and the impact angle constraint is simultaneously satisfied. (2) the faster convergence and deeper search depth are well guaranteed by using MMPSO, so that the optimized weighting matrices with higher accuracy can be obtained rapidly; (3) optimal control of guidance system, reduced control effort, smoother trajectories, no time-to-go, and high efficiency can be achieved.

This paper is structured as follows. The problem formulation is presented in Section II. The controller design is proposed in Section III. In Section IV the MMPSO algorithm is devoted. Then comparison the method with the other known PSO algorithms in Section V part A, as well as applying the proposed guidance law on tactical interceptor system to validate the theoretical analysis in its part B. The conclusions are offered in Section VI, funding support in Section VII, and declaration of conflicting interests in Section VIII.

2. PROBLEM FORMULATION

The planar interception model is obtained from [23]. Now considering total force on the system, the nonlinear engagement kinematics equations are expressed in the inertial Cartesian coordinate system as follows

$$\begin{cases} \dot{x}_M(t) = V_M \cos\left(\gamma_M(t)\right) \\ \dot{y}_M(t) = V_M \sin\left(\gamma_M(t)\right) \\ \dot{\gamma}_M(t) = -a_M(t)/V_M \end{cases} \tag{1}$$

where V_M is the speed of interceptor and is a constant, $\gamma_M(t)$ is the path angle of interceptor, $a_M(t)$ is the total acceleration and perpendicular to the velocity vector, and $x_M(t)$, $y_M(t)$ are the position coordinates in plane x axis and y axis, respectively.

The linearizing equations of motion around a nominal circular trajectory are received from [33]

$$\begin{cases} \dot{\Delta r}(t) = \Delta v_r(t) \\ \dot{\Delta v}_r(t) = -\Delta u(t) - K_\omega^2 \Delta r(t) \end{cases} \tag{2}$$

where Δr and Δv_r are the deviations of the radius and the radial velocity, respectively. K_ω is the control gain and Δu is the deviation from the nominal acceleration.

Using state space represents Eq. (2), obtain

$$\dot{\Delta x}(t) = \tilde{F}_r \Delta x(t) + \tilde{G}_r \Delta u(t) \tag{3}$$

where

$$\Delta x = [\ \Delta r \quad \Delta v_r\ ]^T;\quad \tilde{F}_r = \begin{bmatrix} 0 & 1 \\ -K_\omega^2 & 0 \end{bmatrix};\quad \tilde{G}_r = \begin{bmatrix} 0 \\ -1 \end{bmatrix} \tag{4}$$

Further discretize Eq. (3) with the sampling interval Δt and receive

$$\Delta x(k+1) = F_r \Delta x(k) + G_r \Delta u(k) \tag{5}$$

where k represents the time index, and the discretized matrices are obtained by $F_r = e^{\Delta t \tilde{F}_r}$ and $G_r = \left(\int_0^{\Delta t} e^{\tau \tilde{F}_r}\, d\tau\right)\tilde{G}_r$. The linear quadratic objective function is

$$\begin{cases} \min\limits_{u_0,\cdots,u_{N-1}} \sum\limits_{k=0}^{N-1} \left(\Delta x_k^T Q_k \Delta x_k + \Delta u_k^T R_k \Delta u_k\right) + \Delta x_N^T Q_N \Delta x_N \\ subject\ \text{to}\ \ \Delta x_{k+1} = F_r \Delta x_k + G_r \Delta u_k \end{cases} \tag{6}$$

where the weighting matrices satisfy $Q_0, \cdots, Q_N \geq 0$ and $R_0, \cdots, R_{N-1} > 0$, and the values of both the matrices are

real-time gains with Δx_k and Δu_k. The length of the horizon N is equal to $N = t_f / \Delta t$.

3. CONTROLLER DESIGN

Here the optimization problem is solved analytically by discrete DP algorithm. Its proof was stated clearly in [30], as Hamilton-Jacobi-Bellman equation and Shur complement theorem were employed thus the proof process was simpler than the original. Theorem about optimal controller as following:

Theorem 1 (Optimal controller): Suppose $Q_0,\cdots,Q_N \geq 0$ and $R_0,\cdots,\mathrm{R}_{N-1} > 0$, and consider the following convex optimization problem under affine dynamic constraints with F_r and G_r. For Eq. (6), the optimal solution is affine in Δx and is explicitly given by

$$\Delta u_k = K_k \Delta x_k \tag{7}$$

where the control gain is given by

$$K_k = -\left(G_r^T P_{k+1} G_r + R_k\right)^{-1} G_r^T P_{k+1} F_r \tag{8}$$

with

$$P_k = Q_k + F_r^T P_{k+1} F_r - F_r^T P_{k+1} G_r \left(G_r^T P_{k+1} G_r + R_k\right)^{-1} G_r^T P_{k+1} F_r \tag{9}$$

We know that P_k is computed by backward recursion from $P_N = Q_N$, and the optimal solution of the problem in Eq. (6) can be obtained via solving a series of discrete Riccati equations.

Remark 1: the performance of this guidance depends on the choose of weighting matrices Q_k and R_k. Here K_k is used to control the dynamic response and precision of controller. Moreover, both the matrices and the preceding optimal gain matrix K_k can be computed offline and tabulated in the flight computer.

4. MMPSO ALGORITHM

A. MMPSO Objective Function

The optimization objective function is set at Eq. (10), which includes two parts: the minimum deviation of radius and radial velocity at the end, as well as the minimum control effort during the whole process.

$$J = \Delta x_N^T Q_N \Delta x_N + \sum_{\tau=k}^{N-1} \left(\Delta u_\tau^T R_\tau \Delta u_\tau\right) \tag{10}$$

B. MMPSO Algorithm

As we say before, MMPSO primarily improves the particle swarm searching mode, exactly three searching modes are employed by each particle to seek the local or global best solution, while they adjust the modes timely according to the dynamic environment. The concrete improvements, particle swarm searching mode and its adjustment, are shown as following.

1. searching mode

a. Roam mode. We call the particle carries out the activities in roam mode at k moment if the particle fly to the individual historical best pb_{id}^k and take the search activity around it. The update equations of particle velocity and position as following:

$$\begin{cases} v_{id}^{k+1} = c_1 \cdot r_1 \cdot v_{id}^k + c_2 \cdot r_2 \cdot pb_{id}^k \\ x_{id}^{k+1} = x_{id}^k + v_{id}^{k+1} \end{cases} \tag{11}$$

where i is the sequence number of particle p_i, $i = 1,2,\cdots,N$; k is the number of iteration time, $k = 1,2,\cdots,m$; d is the dimension of solution space, $d = 1,2,\cdots,D$; c_1 and c_2 are the learning factors, r_1 and r_2 are the two random number and obey uniform distribution in $[0,1]$. v_{id}^k is the d dimension speed of particle p_i after k iteration times, also x_{id}^k is the d dimension position of particle p_i after k iteration times.

b. Search mode. The particle search activities not only consider the pb_{id}^k up to now but also the global best gb_d^k of the whole search space is taken into account at k moment. The update equations of particle velocity and position for this case as following:

$$\begin{cases} v_{id}^{k+1} = w_k v_{id}^k + c_1 \cdot r_1 \cdot \left(pb_{id}^k - x_{id}^k\right) + c_2 \cdot r_2 \cdot \left(gb_d^k - x_{id}^k\right) \\ x_{id}^{k+1} = x_{id}^k + v_{id}^{k+1} \end{cases} \tag{12}$$

where inertia weight coefficient w_k needs to meet $0 < w_{\min} < w_k < w_{\max}$, both w_{min} and $w_{\max}$ are the constants. There is $w_k = w_{\max} - \left(w_{\max} - w_{\min}\right) k / K$ in simulation experiment, where k is the current optimal times and K is the total optimal times.

c. Forage mode. The particles fly to gb_d^k just around it from different directions and do the search activities at

k moment. Differently, just update the particle position, the equation as following, yet particle velocity is not changed.

$$x_{id}^{k+1} = gb_d^k \tag{13}$$

2. Searching Mode Adjustment

It is known that a bird transfers information to another by birdsong thus the three tasks should be finished in advance:

Decide the information sender. Assuming the population size is M and the position of particle p_i is x_{id}^k at k moment. Ranking the whole particles in accordance with their fitness values from the best to the worst, and denote as r_{ik} at k moment, thus we have $1 \le r_{ik} \le M$. When $r_{ik} = 1$, particle p_i locates the best position at k moment, similarly it locates the worst position when $r_{ik} = M$. Therefore, the smaller r_{ik} the easier particle is to be the sender.

Design the rule of receiving information. The definition of the minimum strength for receiving information, when particle p_i locates on the x_{id}^k at k moment. That is

$$s_{ik} = \frac{r_{ik} - 1}{M - 1} \tag{14}$$

where $0 \le s_{ik} \le 1$ and $s_{ik} \le s_{jk}$, $i, j = 1,2,\cdots,\mathrm{M}$. We know that the larger probability of particle p_i receiving the information the smaller s_{ik}.

Adjust the searching mode. Denote φ_k as the signal intensity at k moment and it obeys the uniform distribution in $(0, 1]$. The regulations as following:

i. particle p_i searches food in roam mode if $\varphi_k < s_{ik}$. Which means the particle does not receive the information φ_k at k moment;

ii. particle p_i activities as search mode if $\frac{1}{3}\varphi_k < s_{ik} \le \varphi_k$. Which means the particle receives the information φ_k at k moment rather the information implies no fruits found;

iii. particle p_i searches in the space as foraging mode if if $0 < s_{ik} \le \frac{1}{3}\varphi_k$. Which means the particle receives the information φ_k at k moment as well as the information predicts found fruits.

After all, the information sender is decided and updated timely primarily according to its fitness value, and the search mode adjustment for every particle is constantly changed by the received information strength, also each one activities as its selected mode to seek the global best solution in the whole solution space. Consequently, comparing to other PSO algorithm, MMPSO own better search efficiency and accuracy.

5. SIMULATIONS

This section includes two parts. For one, to show the performance of the MMPSO, this method is used to compare with other four PSO algorithms by eight professional test functions. On the other hand, the proposed HDP guidance law is applied to intercept station target.

A. Comparing MMPSO with other PSO Algorithms

The professional test functions consist of two unimodal functions and six multimodal benchmark functions, which are used to the comparison between the MMPSO and other PSO algorithms. These functions are divided into two groups: unimodal problems and unrotated multimodal problems. Their formulas are presented as following.

Group A: Unimodal and Simple Multimodal Problems

1. Sphere function

$$f_1(x) = \sum_{i=1}^{D} x_i^2 \tag{15}$$

2. Rosenbrock's function

$$f_2(x) = \sum_{i=1}^{D-1}\left(100\left(x_i^2 - x_{i+1}\right)^2 + \left(x_i - 1\right)^2\right) \tag{16}$$

Group B: Unrotated and Multimodal Problems

3. Ackley's function

$$f_3(x) = -20\exp\left(-0.2\sqrt{\frac{1}{D}\sum_{i=1}^{D} x_i^2}\right) - \exp\left(\frac{1}{D}\sum_{i=1}^{D}\cos\left(2\pi x_i\right)\right) + 20 + e \tag{17}$$

4. Griewank's function

$$f_4(x) = \sum_{i=1}^{D}\frac{x_i^2}{4000} - \prod_{i=1}^{D}\cos\left(\frac{x_i}{\sqrt{i}}\right) + 1 \tag{18}$$

5. Weierstrass function

$$f_5(x)=\sum_{i=0}^{D}\left(\sum_{k=0}^{k_{\max}}\left[a^k\cos\left(2\pi b^k\left(x_i+0.5\right)\right)\right]\right)-D\sum_{k=0}^{k_{\max}}\left[a^k\cos\left(2\pi b^k\cdot 0.5\right)\right] \quad (19)$$
$$a=0.5,\qquad b=3,\qquad k_{\max}=20$$

6. Rastrigin's function

$$f_6(x)=\sum_{i=1}^{D}\left(x_i^2-10\cos\left(2\pi x_i\right)+10\right) \quad (20)$$

7. Noncontinuous Rastrigin's function

$$f_7(x)=\sum_{i=1}^{D}\left(y_i^2-10\cos\left(2\pi y_i\right)+10\right)$$
$$y_i=\begin{cases}x_i, & |x_i|<\dfrac{1}{2}\\ \dfrac{round\left(2x_i\right)}{2}, & |x_i|\geq\dfrac{1}{2}\end{cases}\quad \text{for } i=1,2,\cdots,D \quad (21)$$

8. Schwefel's function

$$f_8(x)=418.9829\times D-\sum_{i=1}^{D}x_i\sin\left(\left|x_i\right|^{\frac{1}{2}}\right) \quad (22)$$

The engagement parameters for testing the performance simulation are: x^* is the global optimal and its corresponding fitness value is $f\left(x^*\right)$, as well as the search range of each function is $\left[X_{\min},X_{\max}\right]$. These arguments are given in Table **1**.

Experiments are conducted to compare five PSO algorithms, including PSO, UPSO, FDRPSO, CLPSO and MMPSO algorithms. The population size is set at 30, the iteration number is set at 3000 and Monte Carlo (MC) simulation time is set at 30. The curves of their median convergence characteristics are presented in Figure **1**.

We know from Figure **1** that, the proposed MMPSO has faster convergence and deeper search depth in most cases, i.e., optimized value with higher accuracy can be obtained in short time through this optimization method. This conclusion can also be gained by the simulation data shown in Table **2**.

B. Interceptor again Target Simulation

Here we consider a nonlinear tactical interceptor system against a fixed target. It requires that the interceptor attacks the target with small impact angle and velocity error, and control effort must be the minimum. It is assumed that the impact angle could be estimated within sufficient accuracy via the inertial measurements.

B.1. Design Weighting Factor Matrices

As we know from the fore mentioned that the state and control weighting matrices $Q_i=diag\left(\begin{bmatrix}q_{1i} & q_{2i}\end{bmatrix}\right), i=1,2,\cdots,N$ and $R_j=r_jI$, $j=1,2,\cdots,\mathrm{N}-1$, respectively, have an important impact on the guidance law. Now we design the following time-varying parameters for the two weighting matrices

$$\begin{cases}q_{1i}=q_{1N}e^{-10(\mathrm{N}-i)/N}, q_{2i}=q_{2N}e^{-10(\mathrm{N}-i)/N}, i=1,2,\cdots,N\\ r_j=r_{N-1}, \mathrm{j}=1,2,\cdots,\mathrm{N}-1\end{cases} \quad (23)$$

The exponentially growing terms in Q_k and R_k are designed to achieve small Δr and Δv_r, the peak values at $k=N$ are chosen to provide balanced performance on the terminal constraint satisfaction.

Table 1: Global Optimum search Ranges and Initialization Ranges of the Test Function

Test function	Expected optimal value	Expected optimal function value	Search range
f_1	$[0,0,\cdots,0]$	0	$[-100,100]^D$
f_2	$[1,1,\cdots,1]$	0	$[-2.048,2.048]^D$
f_3	$[0,0,\cdots,0]$	0	$[-32.768,32.768]^D$
f_4	$[0,0,\cdots,0]$	0	$[-600,600]^D$
f_5	$[0,0,\cdots,0]$	0	$[-0.5,0.5]^D$
f_6	$[0,0,\cdots,0]$	0	$[-5.12,5.12]^D$
f_7	$[0,0,\cdots,0]$	0	$[-5.12,5.12]^D$
f_8	$[420.96,420.96,\cdots,420.96]$	0	$[-500,500]^D$

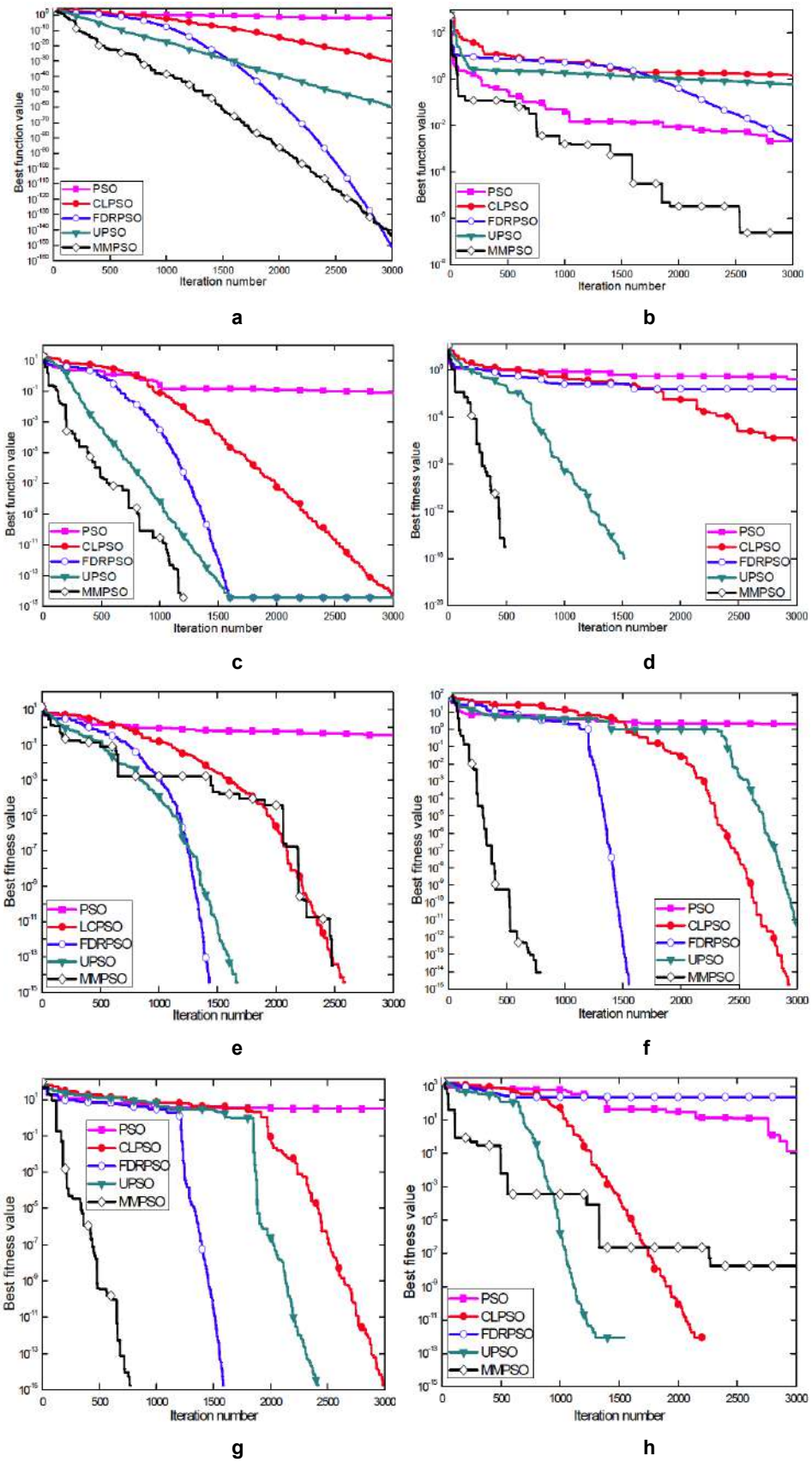

Figure 1: The median convergence characteristics of 10-D test functions. (**a**) Sphere function. (**b**) Rosenbrock's function. (**c**) Ackley's function. (**d**) Griewank's function. (**e**) Weierstrass function. (**f**) Rastrigin's function. (**g**) Noncontinuous Rastrigin's function. (**h**) Schwefel's function.

Table 2: Comparison Test Function Result for PSO Algorithms

Test function	Algorithm	Average Coverage value	Average Coverage value	Test function	Algorithm	Average Coverage value	Average Coverage value
f_1	PSO	0.0192	2931	f_2	PSO	0.0021	2773
	UPSO	6.2442e-61	2997		UPSO	0.6221	2998
	FDRPSO	5.1344e-152	2998		FDRPSO	0.0023	2994
	CLPSO	1.4913e-31	2999		CLPSO	1.5472	2986
	MMPSO	3.1507e-144	2986		MMPSO	2.3526e-07	2537
f_3	PSO	0.0766	2943	f_4	PSO	0.1689	2917
	UPSO	3.5527e-15	1587		UPSO	0	1517
	FDRPSO	3.5527e-15	1587		FDRPSO	0.0246	1680
	CLPSO	3.5527e-15	2985		CLPSO	1.1707e-06	2999
	MMPSO	0	1202		MMPSO	0	491
f_5	PSO	0.3652	2786	f_6	PSO	2.0946	2904
	UPSO	0	1673		UPSO	4.8619e-12	2992
	FDRPSO	0	1432		FDRPSO	0	1551
	CLPSO	0	2589		CLPSO	0	2935
	MMPSO	0	2486		MMPSO	0	794
f_7	PSO	3.1072	2849	f_8	PSO	0.1301	2922
	UPSO	0	2423		UPSO	0	1544
	FDRPSO	0	1591		FDRPSO	236.8767	924
	CLPSO	0	2988		CLPSO	0	2211
	MMPSO	0	772		MMPSO	1.7846e-08	2272

Remark 2: the experiment codes for PSO, UPSO, FDRPSO and CLPSO methods are available from http://www.ntu.edu.sg/home/epnsugan.

The nonlinear kinematics mode in the inertial Cartesian frame is used here. The parameters are as follows: the range from launch point to the stationary target is 5000m, the speed of the interceptor is 200m/s, the desired launch angle and desired impact angle ξ_{des} are equal to 75deg. The heading error (HE) is defined as the difference between the desired and real launch angle, and it equals to 5deg, the acceleration of the interceptor is bounded to 10g (322 m/s^2). Similarly, the parameters of MMPSO algorithm for achieving optimal weighting matrices are as follows: the population size is set at 30, the iteration number is set at 30, the MC is set at 30, the maximum and minimum of inertia weight coefficient w are respectively set at 0.9 and 0.4, the dimension of space is set at 3, the range of particle velocity is $V \in [-2,2]$. Assuming that the optimal components of Q and R in the extremely enormous range, i.e., $q_{1N}, q_{2N}, r_{N-1} \in [0.01, 1e+05]$, the two learning factors are c_1 and c_2, and both of them are equal to 2. The curve about the minimum fitness value is shown in Figure **2**.

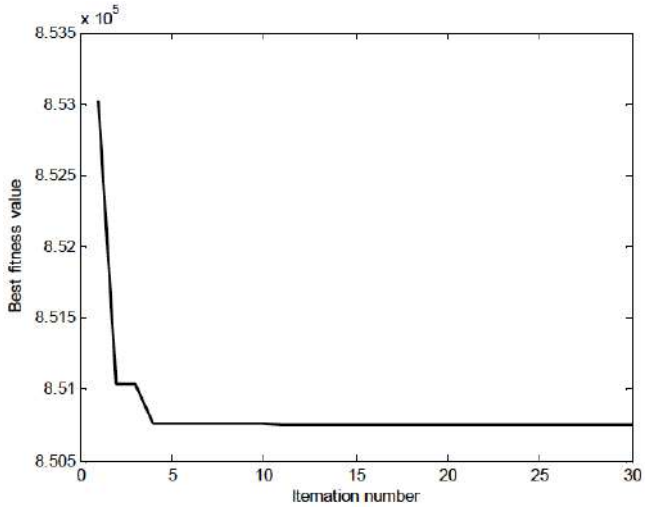

Figure 2: Curve about minimum fitness value.

We can obtain the optimal weight values for q_{1N}, q_{2N} and r_{N-1} from Figure **2**, e.g., 207.0807, 5886.8778 and 6996.2208, respectively. It reveals that the dramatically declined tendency occurs when the iteration number is about three and the fitness value

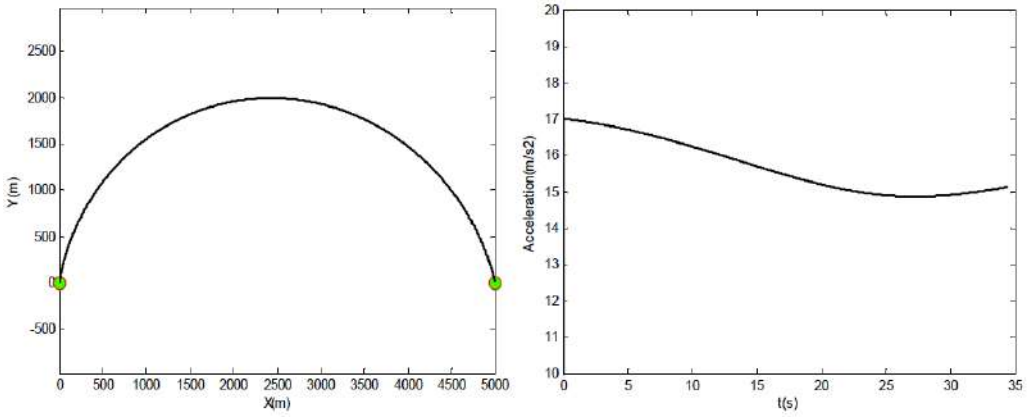

Figure 3: Interceptor trajectory and acceleration simulation for expected impact angle and HE are equal to 75deg and 5deg. (**a**) Interceptor trajectory simulation. (**b**) Acceleration simulation.

tends to converge when the iteration number is about five, i.e., the MMPSO method has the fast converge property. These weight values are used to the proposed HDP guidance and realize the simulations about interceptor trajectory and acceleration with expected impact angle and HE, which are shown in Figure **3**.

Figure **3a** demonstrates that the target can be intercepted successfully when the optimal weight matrices are applied into the proposed guidance law. This means that the obtained weight values are effective and can make the terminal states to reach the expected states, i.e., the expected radius and radial velocity are achieved. On the other hand, we see from Figure **3b** that the control effort is smaller when interceptor is closer to the terminal. This is correspondent to the theory.

Remark 3: the above simulations are an example of applying MMPSO algorithm to obtain the weighting matrices for HDP guidance law. The received weighting matrices values are used to the following sections.

B.2. Effect of Heading Errors

Here we present the nominal trajectories of interceptor from launch point to the target, the two points are denoted by two large dots in Figure **4**, and the different desired impact angles ξ_{des} range from -150deg to 150deg. The two weighting matrices Q_i and R_j are arbitrarily chosen in the range of mentioned before, and we chose q_{1N}, q_{2N}, r_{N-1} are equal to 0.01. As there is no HE existed, the corresponding guidance accelerations are constant and equal to $a_M = V_M^2 / R = 2\left(V_M^2 / D\right)\sin\left(\xi_{des}\right)$ in this case. The curves of nominal trajectories and acceleration for different desired impact angles are shown in Figures **4** and **5**.

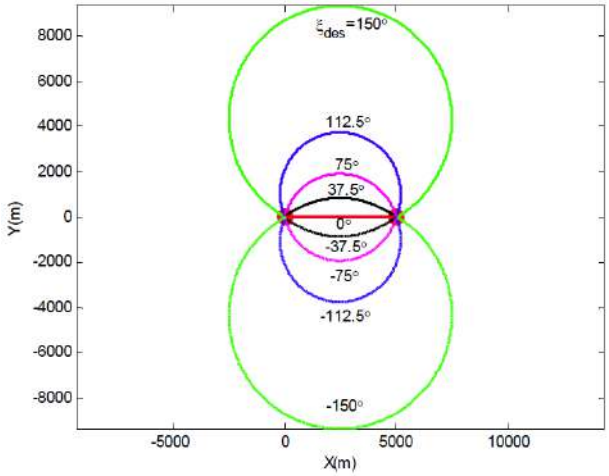

Figure 4: Nominal trajectories for different desired impact angles.

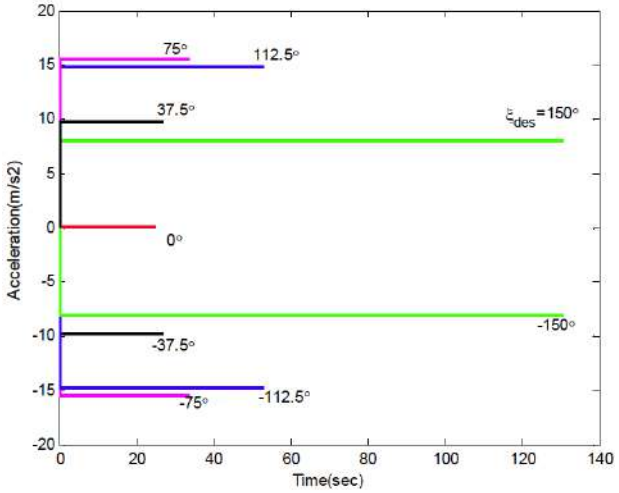

Figure 5: Nominal acceleration for different desired impact angles.

The trajectories and accelerations of interceptor with different HE and the specific expected impact

Table 3: Weight Matrices of Different HE for ξ_{des} are Equal to 0deg and 30deg

		weight matrix value ($\times 10^4$)					weight matrix value ($\times 10^4$)		
$\xi_{des}(deg)$	$HE(deg)$	q_{1N}	q_{2N}	r_{N-1}	$\xi_{des}(deg)$	$HE(deg)$	q_{1N}	q_{2N}	r_{N-1}
0	150	0.1786	1.5600	8.7842	30	120	0.0577	0.6824	7.0015
	112.5	1.4289	1.9327	9.3636		90	0.5535	0.8663	10
	75	4.1119	10	9.0972		60	1.7520	9.9999	9.9999
	37.5	6.2007	10	10		30	2.8246	3.4582	10
	0	0.7574	5.0979	10		0	1E-06	1E-06	10
	-37.5	6.2645	8.7630	10		-30	5.8224	5.9333	10
	-75	3.4159	8.1106	7.5227		-60	7.0129	4.1765	9.7134
	-112.5	0.5441	0.2442	3.7539		-90	5.9364	1E-06	10
	-150	0.0952	0.01	10		-120	2.4801	10	10

ξ_{des} : Desired Impact Angle; HE: Heading Error.

angles (0deg and 30deg) are shown in Figures **6-9**. The expected initial launch angles are equal to the expected impact angles in the following sections. As there are different HE angles, different weighting matrices values are needed. The optimal weighting matrices achieved by MMPSO are displayed in Table **3**.

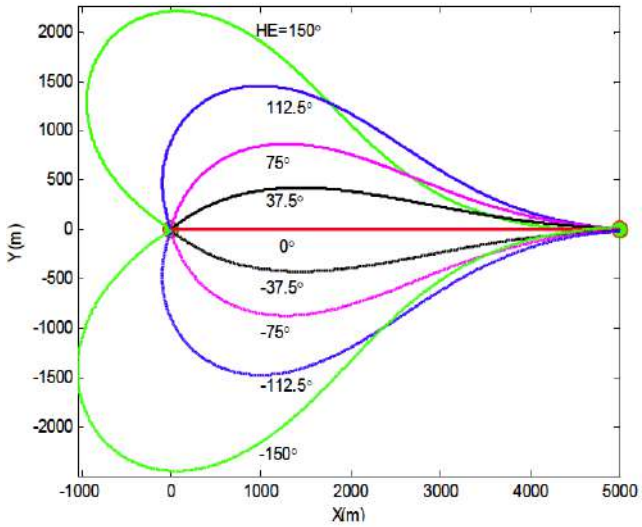

Figure 6: Trajectories with desired impact angle 0deg and different heading errors.

Figures **6** and **8** show that interceptor can hit the target with different expected impact angles under different HE angles. Even though the HE is large, such as ±150 deg with impact angle 0 deg and ±120deg with impact angle 30deg, the aircraft guided by the proposed law can also fulfill the interception. This means that the presented guidance law with the optimized weighting matrices is effective. Furthermore, we can get from their acceleration curves displayed in Figures **7** and **9** that the large guidance accelerations are needed in these cases to realize the attack at the initial phase when there are HE angles in the system. However, the required accelerations can be decreasing over time, and can gradually close to 0. It means that the trajectories can close to the optimal with minimum control effort under the diverse HE angles during the process. Considering that the changes of trajectory and acceleration with both the expected impact angles is basically identical, only the situation that impact angle equals to 30deg is discussed in the following sections.

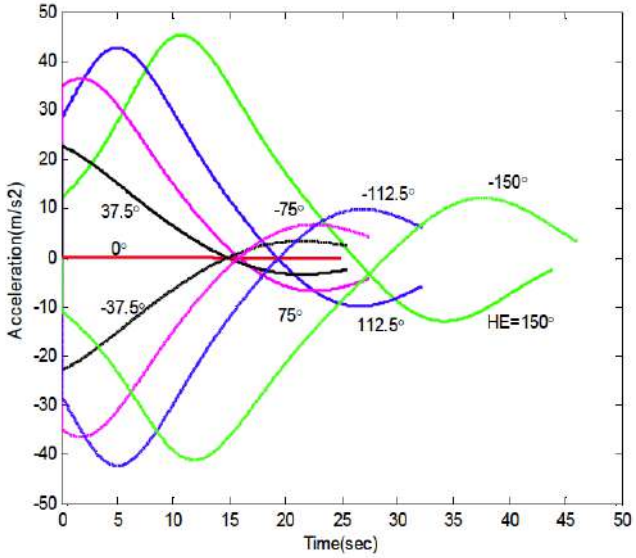

Figure 7: Acceleration with desired impact angle 0deg and different heading errors.

B.3. Analysis of Interceptor Velocity Direction

As γ is the sum of the expected launch angle and HE angle, this angle can be used to analyze the effect

caused by HE angles, and can describe the change of velocity with interceptor in Cartesian coordinates. The curves for γ angle under different HE angles are shown in Figure **10**.

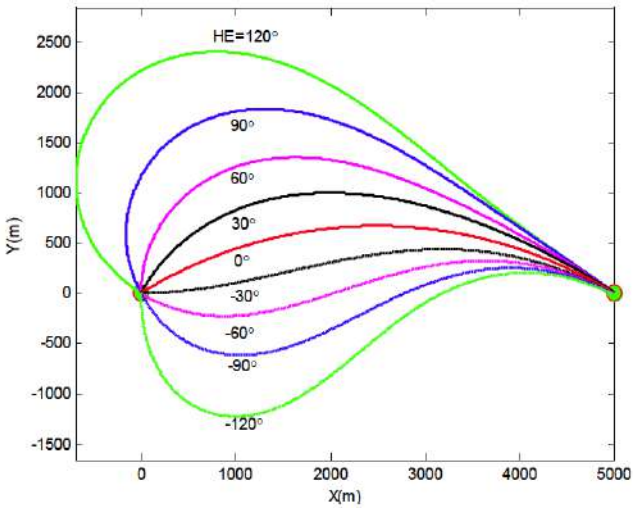

Figure 8: Trajectories with desired impact angle 30deg and different heading errors.

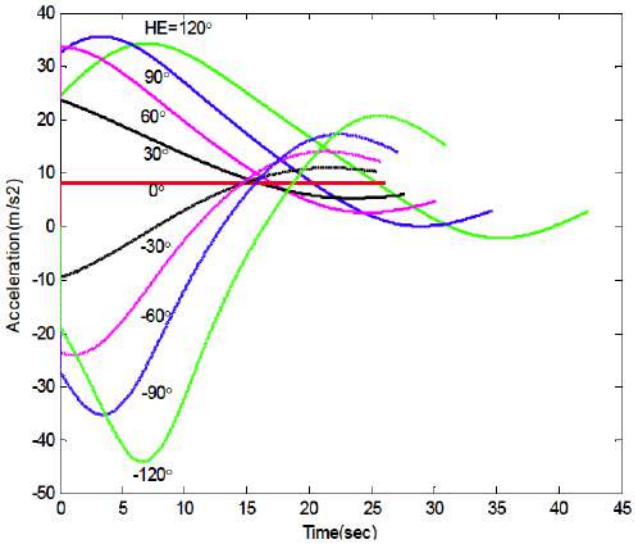

Figure 9: Acceleration with desired impact angle 30deg and different heading errors.

We see from Figure **10** that these curves can converge to the expected impact angle, i.e., 30deg, even though their initial angles are diverse. The change totally agrees with the theoretical analysis. Moreover, it also reflects the validity of the proposed guidance law.

B.4. Analysis of the State Variable and the Deviation of Impact Angle

Δr is the deviation between the real trajectory and its nominal. Similarly, Δv_r and $\Delta\xi$ represent deviation with radial velocity and impact angle, respectively. Here the changes of these three important error variables under the impact of different HE angles are provided and presented in Figures **11-13**.

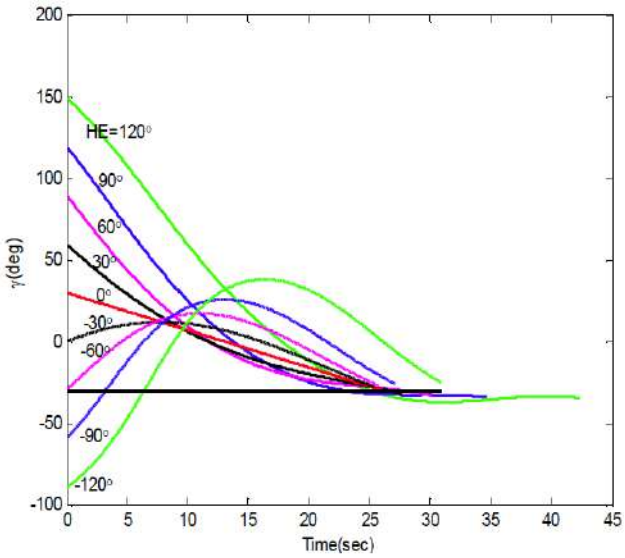

Figure 10: Interceptor velocity direction change with the expected impact angle 30deg.

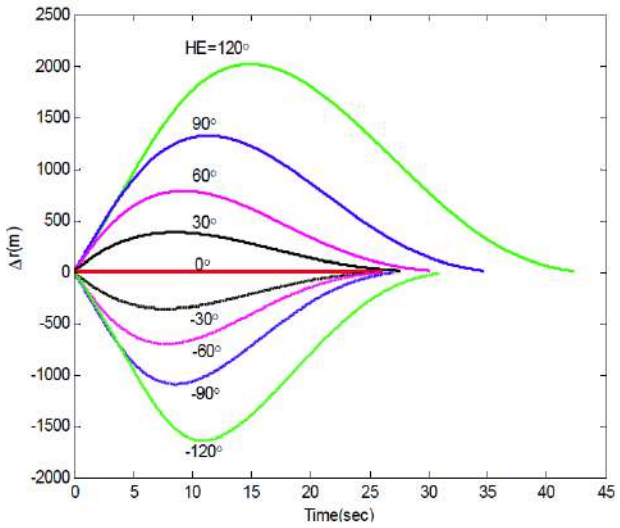

Figure 11: The change of the radius deviation for the expect impact angle 30deg.

We see from Figure **11** that the change of Δr is different from Δv_r and $\Delta\xi$. Especially, Δr is equal to zero under different HE angles at the initial moment, as the interceptor is located in the launch point at that moment, and their real radiuses are equal to the nominal ones. However, the values of Δr are increasing over time and reaching their peak ones, and then tend to zero gradually. This means that this type of error can be reduced at terminal phase. Aside from that, it shows from Figures **12** and **13** that both the Δv_r and $\Delta\xi$ have the identical tendency. Exactly, their values become large at the initial phase due to the HE,

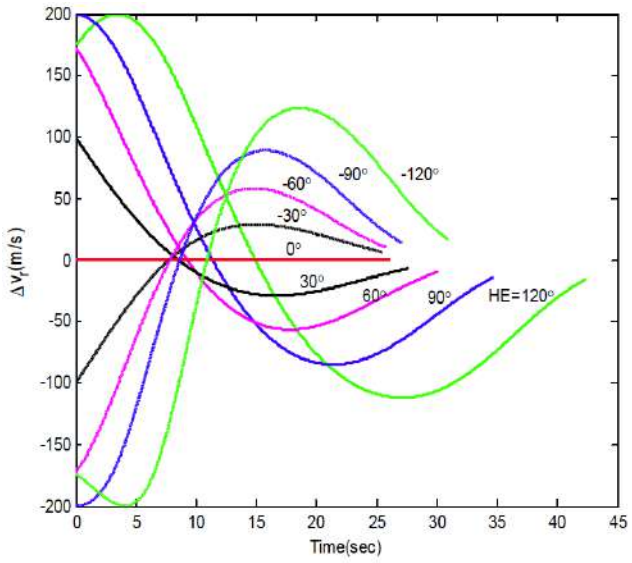

Figure 12: The change of the radial velocity deviation for the expect impact angle 30deg.

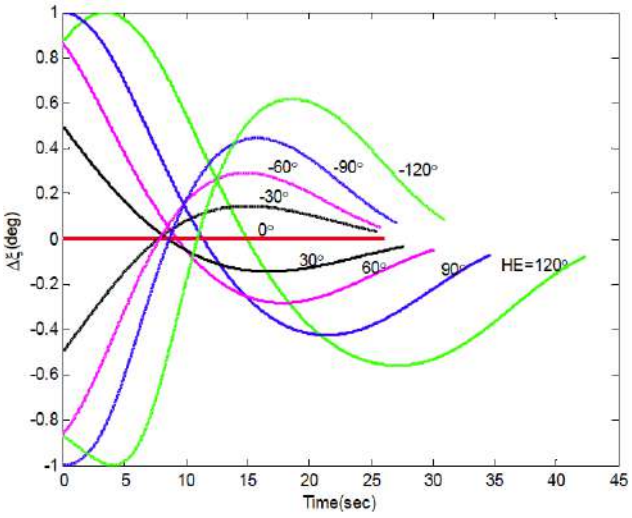

Figure 13: The change of the impact angle deviation for the expect impact angle 30deg.

i.e., the maximum values of Δv_r and $\Delta\xi$ respectively reaches to 200m/s and 1deg when HE equals to 120deg, but the error values can swiftly decline and close to zero when trajectories converge to their nominal ones. It indicates that both types of the errors can also be diminished under the presented guidance law.

B.5. Influence of the Interceptor Dynamics

The comparison of the trajectory and corresponding acceleration between having and without autopilot lag is presented in this section. The autopilot is modeled as first-order dynamics and its transfer function is

$$\frac{a_{real}}{a_{com}} = \frac{1}{\tau_A s + 1} \tag{24}$$

where a_{real} is the real acceleration for interceptor and a_{com} is the command acceleration. The engagement parameters for the situation as follows: the autopilot lag τ_A is set at 1(in seconds), the three desired impact angles are set at 5deg, 40deg and 75deg, and HE is set at 5deg. The weighting matrices for without and having lag are listed in Table **4**. The comparison curves of trajectory and acceleration for these angles are shown in Figures **14** and **15**.

Figures **14** and **15** demonstrate that the trajectory and acceleration curves for lag system approximately coincide with the without ones, especially for at the terminal phase. This means that the proposed guidance law can also be useful for analyzing the lag ones, although there is the minute difference at the initial and middle phases.

B.6. Comparison Between HDP and BPNG

To illustrate the performance of the proposed guidance law, the comparison between this guidance law and BPNG [24] is made in this section. The parameters are as follows: the weighting matrices for HDP are given in Table **5**, the BPNG gain N_{BPNG} and η_{BPNG} are respectively set to 3 and 1, the desired impact angles are in the interval of 5 to 55 deg, and the heading error is equal to 5 deg (for impact angles that are larger than 55deg, the BPNG guidance law diverges and fails to intercept the target). The

Table 4: Weight Matrices for ξ_{des} are Equal to 5 deg, 25 deg and 75 deg and HE is 5 deg

		without lag weight matrix value($\times 10^4$)			with lag weight matrix value ($\times 10^4$)		
$HE(deg)$	$\xi_{des}(deg)$	q_{1N}	q_{2N}	r_{N-1}	q_{1N}	q_{2N}	r_{N-1}
	5	1.7251	10	8.9351	1.4080	4.4086	8.9241
5	40	7.4844	7.7793	9.7533	1.9484	10	10
	75	6.26543	10	10	2.1963	10	10

ξ_{des} : Desired Impact Angle; HE: Heading Error.

simulation results of trajectory, acceleration and control effort are shown from Figures **16-18**, and the control effort values with BPNG and HDP under three HE angles are shown in Table **6**.

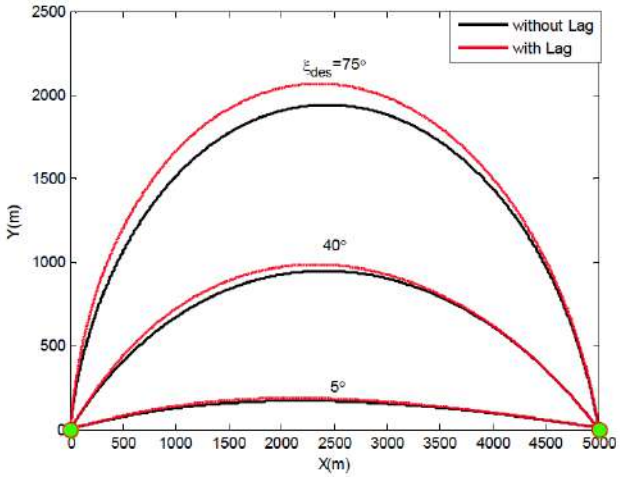

Figure 14: Comparison the trajectory for with/without autopilot lag.

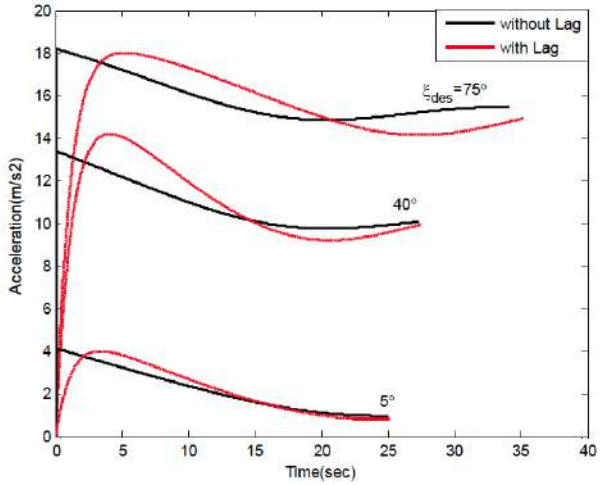

Figure 15: Comparison the acceleration for with/without autopilot lag.

Table 5: Weight Matrices for ξ_{des} are Equal to 5 deg, 30 deg and 55 deg, and HE is 5 deg

		without lag weight matrix value($\times 10^4$)		
HE(deg)	ξ_{des}(deg)	q_{1N}	q_{2N}	r_{N-1}
	5	1.7251	10	8.9351
5	30	8.836	8.7099	8.7800
	55	0.81386	10	2.6584

ξ_{des} : Desired Impact Angle; HE: Heading Error.

From Figure **16**, we see that the two guidance laws can fulfill the interception extremely even when the desired impact angle is large, i.e., 55deg. However, the trajectories of BPNG are more curved than those of

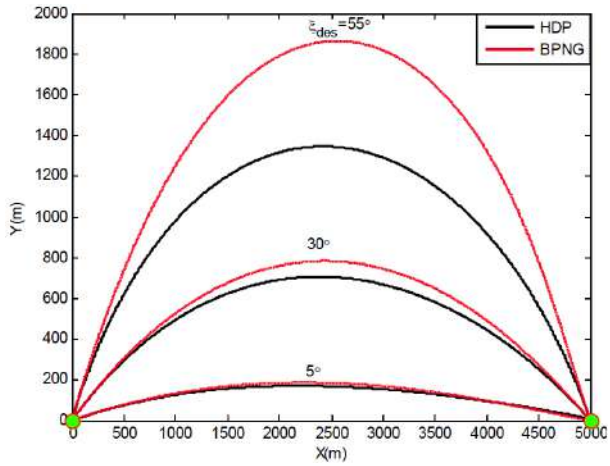

Figure 16: Trajectory comparison between HDP and BPNG.

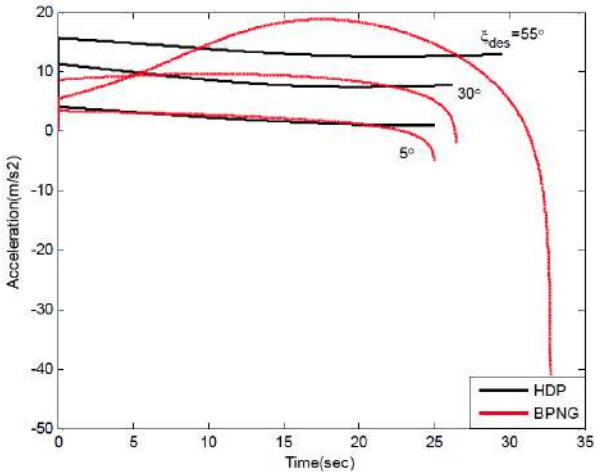

Figure 17: Acceleration comparison between HDP and BPNG.

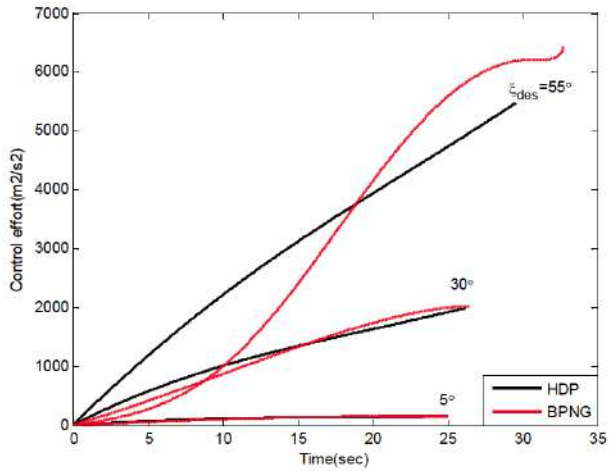

Figure 18: Control effort comparison between HDP and BPNG.

HDP. It indicates that BPNG needs more guidance acceleration compared with the HDP, although both of them are valid. This can be verified by Figure **17**. It shows from this figure that the required guidance accelerations with the proposed HDP are smaller than those of BPNG under three desired impact angle, especially for the large desired impact angle, i.e., 55deg, at the terminal phase. This means that less energy is required by the HDP when intercepting the stationary target. Furthermore, we can obtain the identical conclusion from Figure **18**. It displays that the control effort values with both the laws are basically identical when the impact angles are small, but the larger control effort is needed by BPNG compared with the HDP when the impact angles are large. This can also be acquired by Table **6**. It is shown that the values of control effort with BPNG and HDP are basically equal when HE angles equals to 5deg and 30deg. However, the value with HDP is evidently smaller than BPNG when HE is equal to 55deg, i.e., 8.7398e+6 and 9.9502e+6, respectively.

6. CONCLUSION

This paper presents a new guidance law for circular trajectories. The law is the combination of the MMPSO and HDP algorithm. To fast obtain the two optimized weighting matrices with higher accuracy, MMPSO is used since it has faster convergence and deeper search depth compared with other PSO. On the other hand, to fulfill the optimal control of the guidance system, the HDP method is proposed. Moreover, the weighting matrices acquired from MMPSO are used to design the guidance law based on HDP, so that the fixed target can be attacked successfully, and the desired impact angle can well be satisfied. Besides, the presented law has the following advantages: reduced control effort, smoother trajectories, and high efficiency. These advantages can be validated through simulations.

Table 6: The Comparison of Control Effort between BPNG and HDP under Three HE Angles

HE(deg)	BPNG (m^2/s^2)	HDP (m^2/s^2)
5	2.5796e+5	2.6456e+5
30	2.9825e+6	3.0186e+6
55	9.9502e+6	8.7398e+6

FUNDING

This work was supported by the National Natural Science Foundation of China (Grant Nos. 61463029 and 61308120) and the Postdoctoral Science Foundation of China (Grant Nos. 2013M540783). The authors gratefully acknowledge all of the support.

DECLARATION OF CONFLICTING INTERESTS

The author(s) declared non potential conflicts of interest with respect to the research, authorship, and/or publication of this article.

REFERENCES

[1] Eberhart RC, Kennedy J. A New Optimizer Using Particle Swarm Theory. in Proc. 6th Int Symp Micromachine Human Sci Nagoya, Japan 1995; 39-43. https://doi.org/10.1109/MHS.1995.494215

[2] Kennedy J, Eberhart RC. Particle Swarm Optimization. in Proc. IEEE Int Conf Neural Networks 1995; 4(8): 1942-1948. https://doi.org/10.1109/ICNN.1995.488968

[3] Fan Y, Chi Q, Fang XH, *et al*. State-of-Charge Estimation of Lithium-Ion Batteries Using an Adaptive Particle Filter Based on an Improved Particle Swarm Optimization Algorithm. IEEE Trans Transp Electrification 2025; 11(4): 9428-9438. https://doi.org/10.1109/TTE.2025.3548636

[4] Harkati L. Snowpack Permittivity Retrieval Using Particle Swarm Optimization Algorithm. IEEE Geosci Remote Sens. Lett 2025. https://doi.org/10.1109/LGRS.2025.3587507

[5] Jin HW, Yue GW. Underwater Manipulator Trajectory Planning Based on Improved Particle Swarm Optimization Algorithm. J Field Rob 2025; 42(7): 3986-4008. https://doi.org/10.1002/rob.22603

[6] Ling R, Zhang ZW, Xuan XF. Dual-Frequency Power Amplifiers' Design Based on Improved Multiobjective Particle Swarm Optimization Algorithm. IEEE Microwave Wireless Technol Lett 2025; 35(11): 1768-1771. https://doi.org/10.1109/LMWT.2025.3592184

[7] Wang H, Cai T, Pedrycz W. Kriging Surrogate Model-Based Constraint Multiobjective Particle Swarm Optimization Algorithm. IEEE Trans Cybern 2025; 55(3): 1224-1237. https://doi.org/10.1109/TCYB.2024.3524457

[8] He Q, Yan X, Alireza J, *et al.* Influence Maximization in Sentiment Propagation With Multisearch Particle Swarm Optimization Algorithm. IEEE Trans Comput Social Syst 2025; 12(3): 1365-1375. https://doi.org/10.1109/TCSS.2025.3528890

[9] Zhu DL, Shen JY, He JL, *et al.* Group Merging Particle Swarm Optimization Algorithm for Rural Base Station Deployment. IEEE Trans Emerging Top Comput Intell 2025. early access. https://doi.org/10.1109/TETCI.2025.3558433

[10] Zhang CZ, Wang Y, Li HB. Particle Swarm Optimization by Multi-Search Modes. Journal of Guilin University of Technology 2016; 36(2): 402-409.

[11] Hull DG, Speyer JL, Burris DB. A Linear-Quadratic Guidance Law for Dual Control of Homing Interceptors. AIAA Guidance, Navigation, and Control Conference AIAA, Monterey, California, DC, 1990; 13(1): 137-144. https://doi.org/10.2514/3.20527

[12] Riggs TL, Vergez PL. Advanced Air-to-Air Interceptor Guidance Using Optimal Control and Estimation. AFATLTR-81-56, Air Force Armament Laboratory, 1981.

[13] Rusnak I. Optimal Guidance Laws with Uncertain Time-of-Flight. IEEE Transactions on Aerospace and Electronic Systems 2000; 36(2): 721-725. https://doi.org/10.1109/7.845272

[14] Zhu YJ, Zhou C, Chen S, *et al.* A Parameterized Solution to Optimal Guidance Law Against Stationary Target With Impact Angle Constraint. IEEE Trans Aerosp Electron Syst 2025; 61(2): 3993-4003. https://doi.org/10.1109/TAES.2024.3501996

[15] Cheng L, Wang H, Gong SP, *et al.* Neural-Network-Based Nonlinear Optimal Terminal Guidance With Impact Angle Constraints. IEEE Trans Aerosp Electron Syst 2024; 60(1): 819-830. https://doi.org/10.1109/TAES.2023.3328576

[16] Gong M, Zhou ST, Zhou D. Optimal Sliding Mode Guidance Law Against Maneuvering Target With Impact Angle Constraint. Proc Inst Mech Eng Part G- J Aerosp Eng 2024; 238(5): 513-528. https://doi.org/10.1177/09544100241233327

[17] Zhu JW, Su DL, Xie Y, *et al.* Impact Time and Angle Control Guidance Independent of Time-to-go Prediction. Aerosp Sci Technol 2019; 86: 818-825. https://doi.org/10.1016/j.ast.2019.01.047

[18] Wu FC, Chen Z, Shao XM, *et al*. Nonlinear Optimal Guidance with Constraints on Impact Time and Impact Angle. Autom 2025; 181. https://doi.org/10.1016/j.automatica.2025.112500

[19] Padhi R, Kothari M. Model Predictive Static Programming: A Computationally Efficient Technique for Suboptimal Control Design. Int J Innovative Comput Inf Control 2009; 5(2): 399-411.

[20] Harshal BO, Radhakant P. Impact-Angle-Constrained Suboptimal Model Predictive Static Programming Guidance of Air-to-Ground Interceptors. Journal of Guidance Control and Dynamics 2012; 35(1): 153-164. https://doi.org/10.2514/1.53647

[21] Bhitre N, Achintya KS, Radhakant P. Three-dimensional Impact Angle Constrainted MPSP Guidance of Air-to-Air Interceptors. IEEE International Conference on Control Applications Part of IEEE Multi-Conference on System and Control Hyderabad, India, 2013; 883-888. https://doi.org/10.1109/CCA.2013.6662862

[22] Arnab M, Harshal BO, Radhakant P. Generalized Model Predictive Static Programming and Its Application to 3D Impact Angle Constrained Guidance of Air-to-Surface Interceptors. American Control Conference ACC Washington USA, 2013; 17-19.

[23] Tsalik R, Shima T. Inscribed Angle Guidance. Journal of Guidance Control and Dynamics 2015; 38(1): 30-40. https://doi.org/10.2514/1.G000468

[24] Kim B, Lee J, Han H. Biased PNG Law for Impact with Angular Constraint. IEEE Transactions on Aerospace and Electronic Systems 1998; 34(1): 277-288. https://doi.org/10.1109/7.640285

Received on 20-11-2025 Accepted on 18-12-2025 Published on 31-12-2025